OPEN ACCESS

University of Dundee

University of Dundee

Influence of cement type on resistance to attack from two carboxylic acids

Dyer, Thomas

Published in:
Cement and Concrete Composites

DOI:
10.1016/j.cemconcomp.2017.07.004

Publication date:
2017

Licence:
CC BY-NC-ND

Document Version
Peer reviewed version

Link to publication in Discovery Research Portal

Citation for published version (APA):
Dyer, T. (2017). Influence of cement type on resistance to attack from two carboxylic acids. *Cement and Concrete Composites*, *83*, 20-35. https://doi.org/10.1016/j.cemconcomp.2017.07.004

General rights
Copyright and moral rights for the publications made accessible in Discovery Research Portal are retained by the authors and/or other copyright owners and it is a condition of accessing publications that users recognise and abide by the legal requirements associated with these rights.

• Users may download and print one copy of any publication from Discovery Research Portal for the purpose of private study or research.
• You may not further distribute the material or use it for any profit-making activity or commercial gain.
• You may freely distribute the URL identifying the publication in the public portal.

Take down policy
If you believe that this document breaches copyright please contact us providing details, and we will remove access to the work immediately and investigate your claim.

Download date: 05. May. 2023

© 2017. This manuscript version is made available under the CC-BY-NC-ND 4.0 license
http://creativecommons.org/licenses/by-nc-nd/4.0/

Title: Influence of cement type on resistance to attack from two carboxylic acids.

Thomas Dyer[a]

[a]Concrete Technology Unit

Division of Civil Engineering

University of Dundee

DD1 4HN

UK

t.d.dyer@dundee.ac.uk

ABSTRACT

In a number of circumstances, concrete may be required to possess resistance to organic acids. These are frequently carboxylic acids. This paper examines the effect of two such acids – acetic and butyric – on hardened cement paste specimens made from three cement types – Portland cement (PC), a combination of PC and fly ash (PC/FA), and a calcium sulfoaluminate cement (CSA). Specimens were exposed to solutions of the acids and deterioration characterized in terms of mass loss and pH measurements, micro-CT scanning, and chemical and mineralogical analysis. Additionally geochemical modelling was used to further examine the mechanisms involved during acid attack. The CSA cement was most resistant to attack, with the PC paste displaying the least resistance. This resistance has been partly attributed to the higher acid neutralization capacity of CSA cement. However, this paper demonstrates that the enhanced performance is most probably the result of a denser microstructure.

KEYWORDS

acid attack; Portland cement; fly ash; calcium sulfoaluminate cement; acetic; butyric.

1. INTRODUCTION

Acid resistance is a durability requirement for concrete in a number of applications. In many instances, the acids involved arise from biogenic sources, where heterotrophic microorganisms break down compounds into smaller molecules, many of which are organic acids. Where the micro-organisms are bacteria the organic acid molecules produced are typically, but not always, carboxylic acids with the structural form $CH_3(CH_2)_xCOOH$, where x is a value equal or greater than 0. The handling and storage of animal manure and silage in agricultural applications are two activities in which organic acids arise in such a way [1]. In other instances, organic acids arise from the handling and processing of foodstuffs. Cement used in downhole oilwell applications may also encounter such compounds, which are the result of thermal degradation of hydrocarbons.

There is usually a need to limit the rate at which concrete in contact with such acids deteriorates. The process of deterioration through acid attack can occur through dissolution, a combination of dissolution and complex formation, and fragmentation resulting from the precipitation of expansive salts. In the case of the carboxylic acids produced by bacterial activity, precipitation of salts is not usually encountered, although complex formation resulting from complex formation between the organic molecules and metal ions present in cement hydrates may play a role.

The process of acid attack of a Portland cement-based material where dissolution is the main mode of deterioration initially involves leaching of calcium hydroxide (portlandite):

$$Ca(OH)_2 + 2H^+ \rightarrow Ca^{2+} + 2H_2O$$

Thus, the acid is neutralized by portlandite.

When the Portlandite has been dissolved, the C-S-H phases begins to also lose calcium until all that remains is essentially an amorphous silica gel, possibly containing some aluminium. Since attack involves the ingress of external acidic species, it is common for two layers to form [2]. An outer layer will be observed where the pH is lowest and complete decalcification has occurred. Further beneath the surface, a second layer will form where pH is in transition and only leaching of portlandite has occurred. Beyond this layer is unaffected cement paste whose pore fluids have a high pH. The silica gel layer typically shrinks considerably on drying, and is prone to cracking when this occurs.

In the case of calcium aluminate cements, the process of deterioration is somewhat different. Firstly, calcium hydroxide is absent from most of these cements, and so, whilst decalcification occurs, it is the hydration products C_3AH_6 in converted calcium aluminate cement - or CAH_{10} and C_2AH_8 in the unconverted material – which are involved. Again, the acid is neutralized during the reaction, but this occurs in two stages. Thus, for C_3AH_6 the first stage involves decalcification:

$$Ca_3Al_2O_9.6H_2O + 6H^+ \rightarrow 3Ca^{2+} + 2Al(OH)_3 + 6H_2O$$

The second stage occurs as more acid enters the cement matrix the pH drops further until a sufficiently low pH is reached where $Al(OH)_3$ undergoes amphoteric dissolution [3]:

$$2Al(OH)_3 + 6H^+ \rightarrow 2Al^{3+} + 6H_2O$$

Thus, calcium aluminate cements have a higher acid neutralization capacity [3], which will provide enhanced resistance to acid attack. Additionally, the dissolution of $Al(OH)_3$ under low pH conditions and its subsequent precipitation as a result of the diffusion of aluminium further into the paste where pH is higher, has been identified as producing microstructures which are likely to reduce porosity and act to limit ingress of acidic species [3].

In the case of calcium sulfoaluminate cements, the hydration products will be different, with calcium sulfoaluminate hydrate phases such as ettringite normally being present. However, the reaction with acids remains essentially the same.

This paper examines the performance of three cement types with respect to their performance when exposed to two monocarboxylic acids – acetic and butyric. A secondary objective was to identify any

influence of the difference in acid type on their action on cement. Moreover, the process of acid attack was modelled using geochemical modelling techniques to examine the likely reasons for any differences in behaviour. The characteristics of acetic and butyric acid are discussed in the following section.

1.1 Acetic and butyric acid

Acetic and butyric acid are of comparable strength, indicated by their similar acid dissociation constants (pK_a, Table 1).

Table 1. Acid dissociation constants for acetic and butyric acid.

ACID	FORMULA	ACID DISSOCIATION CONSTANT	REF
		pK_a	
Acetic acid	CH_3COOH 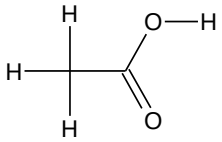	4.76	[6]
Butyric acid	$CH_3CH_2CH_2COOH$ 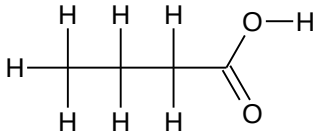	4.82	[7]

In the context of this study, and with particular reference to geochemical modelling of acid attack, the chemical interaction of the two acids with cement is best examined in terms of the complexes formed in aqueous solution and elements found in significant quantities in cement (Ca, Al, Fe and Si), and any reaction products which may be precipitated. In terms of complex formation, the nature of such interactions is characterized using stability constants.

The acetate ion forms weak complexes with Ca, Al and Fe(II) ions, but forms stronger complexes with Fe(III). The stability constants of these complexes are provided in Table 2. The butyrate ion forms complexes with Ca and Al of similar strength to those of the acetate ion. However, there is little evidence in the literature of complex formation between the butyrate ion and iron [4]. One study has identified a basic iron (III) butyrate ion, but based on the influence of butyric acid on iron solubility [5], it would appear that any such complexes are likely to be relatively weak. There are no known complexes formed between Si and either of the organic ions.

In the case of solid reaction products - with regards to acid attack - it is the solubility of such salts which is of key importance, since this will define whether the cement matrix will be dissolved or re-precipitated as a solid salt. Precipitation may also act to alter the nature of the microstructure of the degraded layers, which may have implications for mass transport rates. In some cases, precipitation of salts with a higher molar volume than the original hydration product involved in their formation can lead to fragmentation. The solubilities of salts formed are expressed in Table 3 as solubility products. The salts are relatively soluble. However, iron (III) diacetate and aluminium diacetate are described as insoluble, although no quantitative data could be located in the literature. For this

reason, Table 3 contains assumed solubility constants for these compounds (in brackets) based on the upper limit of the solubility range normally defined for 'insoluble' (<0.1 g/l).

Table 2. Stability constants of complexes formed by calcium, aluminium and iron (II) and (III) ions in water containing acetic and butyric acid. All values are for 25 °C.

COMPLEX	REACTION	STABILITY CONSTANT	REF.
Acetic Acid			
Ca			
	$Ca^{2+} + CH_3CO_2^- \rightleftharpoons Ca(CH_3CO_2)^+$	1.18	
Al			
	$Al^{3+} + CH_3CO_2^- \rightleftharpoons Al(CH_3CO_2)^{2+}$	1.51	
Fe(II)			[7]
	$Fe^{2+} + CH_3CO_2^- \rightleftharpoons Fe(CH_3CO_2)^+$	1.40	
Fe(III)			
	$Fe^{3+} + CH_3CO_2^- \rightleftharpoons Fe(CH_3CO_2)^{2+}$	4.02	
	$Fe^{3+} + 2CH_3CO_2^- \rightleftharpoons Fe(CH_3CO_2)_2^+$	7.57	
	$Fe^{3+} + 3CH_3CO_2^- \rightleftharpoons Fe(CH_3CO_2)_3$	9.59	
Butyric Acid			
Ca			
	$Ca^{2+} + CH_3CH_2CH_2CO_2^- \rightleftharpoons Ca(CH_3CH_2CH_2CO_2)^+$	0.94	[7]
Al			
	$Al^{3+} + CH_3CH_2CH_2CO_2^- \rightleftharpoons Al(CH_2(OH)CO_2)^{2+}$	1.58	

2. MATERIALS AND METHODS

Evaluation was conducted using mass loss measurements on cement paste specimens submerged in acid solutions, and pH measurements of the solutions. At the end of the exposure period, the nature of deterioration was examined using micro-CT imaging of the specimens and powder X-ray diffraction and X-ray fluorescence analysis of the degraded surface layer. The mechanisms of deterioration were further explored using geochemical modelling.

The experimental approach adopted for the study was to allow the acid solution to change as a result of interaction with the specimen – i.e. the solution was not discarded and replenished at intervals. This approach was adopted because it permits the neutralization of acids by the cement paste to be observed, since the neutralization of a finite quantity of acid by the cement will manifest itself in the form of an abrupt increase in pH. The time of occurrence of this event can be used as a means of calibrating geochemical models of acid attack. Additionally, the specimens were allowed to deteriorate without removing the degraded layer. The use of abrasion to remove the degraded layer allows for a reasonably unambiguous assessment of the rate of deterioration through mass loss measurements. However, the approach is indifferent to any influence the degraded layer has on the rate of deterioration, and also makes analysis of this layer difficult.

Table 3. Solubility and molar volume data for compounds relevant to the interaction of hydrated Portland cement with acetic and butyric acid. All values are for 25 °C. Values in brackets are assumed based on qualitative descriptions of compound solubility.

COMPOUND	FORMULA / REACTION	SOLUBILITY PRODUCT, log K_{sp}	REF.	MOLAR VOLUME, cm^3/mol	REF.
Acetate compounds					
Calcium diacetate monohydrate	$Ca(CH_3CO_2)_2.H_2O \rightleftharpoons Ca^{2+} + 2CH_3CO_2^- + H_2O$	1.38	[8]	117	[9]
Calcium diacetate dihydrate	$Ca(CH_3CO_2)_2.2H_2O \rightleftharpoons Ca^{2+} + 2CH_3CO_2^- + 2H_2O$	1.76	[10]	unknown	
Calcium hydrogen triacetate monohydrate	$CaH(CH_3CO_2)_3.H_2O \rightleftharpoons Ca^{2+} + CH_3COOH + 2CH_3CO_2^- + H_2O$	3.07	[10]	158	[11]
Aluminium triacetate	$Al(CH_3CO_2)_3 \rightleftharpoons Al^{3+} + 3CH_3CO_2^-$	'Soluble'	[12]	unknown	
Aluminium diacetate	$Al(CH_3CO_2)_2OH \rightleftharpoons Al^{3+} + 2CH_3CO_2^- + OH^-$	'Insoluble' (-12.24)	[6]	unknown	
Aluminium monoacetate	$Al(CH_3CO_2)OH_2 \rightleftharpoons Al^{3+} + CH_3CO_2^- + 2OH^-$	Assumed to be soluble		unknown	
Iron (II) acetate	$Fe(CH_3CO_2)_2.4H_2O \rightleftharpoons Fe^{2+} + 2CH_3CO_2^- + 4H_2O$	'Soluble'	[6]	127	[13]
Iron (III) diacetate	$Fe(CH_3CO_2)_2OH \rightleftharpoons Fe^{3+} + 2CH_3CO_2^- + OH^-$	'Insoluble' (-12.52)	[6]	unknown	
Butyrate compounds					
Calcium butyrate monohydrate	$Ca(CH_3CH_2CH_2CO_2)_2{\cdot}H_2O \rightleftharpoons Ca^{2+} + 2CH_3CH_2CH_2CO_2^- + H_2O$	0.04	[14]	179	[15]
Aluminium butyrate	$Al(CH_3CH_2CH_2CO_2)_3 \rightleftharpoons Al^{3+} + 3CH_3CH_2CH_2CO_2^-$	Assumed soluble		unknown	
Iron (II) butyrate	$Fe(CH_3CH_2CH_2CO_2)_2 \rightleftharpoons Fe^{2+} + 2CH_3CH_2CH_2CO_2^-$	Assumed soluble		unknown	
Iron (III) butyrate	$Fe(CH_3CH_2CH_2CO_2)_3.3H_2O \rightleftharpoons Fe^{3+} + 3CH_3CH_2CH_2CO_2^- + 3H_2O$	Assumed soluble		unknown	

2.1 Cements

The study examined three cement types: Portland cement (PC), a combination in this case of 65% by mass Portland cement and 35% fly ash (PC/FA), plus a calcium sulfoaluminate (CSA) cement.

The composition of these cements is shown in Table 4.

Table 4. Major oxide composition of the cements used in the study.

	% by mass		
CONSTITUENT	PC	PC/FA	CSA
CaO	67.80	47.17	44.38
SiO_2	20.67	28.94	10.71
Al_2O_3	4.16	9.44	31.75
Fe_2O_3	2.87	5.18	2.23
MgO	1.17	1.61	1.42
Na_2O	0.23	0.34	0.07
K_2O	0.61	1.07	0.28
TiO_2	0.41	0.60	1.47
MnO	0.05	0.06	0.02
P_2O_5	0.16	0.29	nd
SO_3	3.418	3.812	8.695
Cl	0.083	0.114	0.032

nd = not detected.

2.2 Preparation of cement paste specimens

Cement paste specimens were prepared with a water / cement ratio of 0.5 using distilled water. They were mixed by hand for a period of three minutes and poured into polyethylene cylinders with an internal diameter of 22 mm and a height of 70 mm. The cylinders were gently vibrated to remove as many air bubbles as possible. The cylinders were sealed and stored at 25 °C for a period of 28 days.

2.3 Acid solutions and exposure measurements

Each cement specimen was exposed individually to a 4 litre acid solution. The solutions were held in polyethylene tanks with a capacity of 5 litres. Reagent grade acetic and butyric acids were used. Acid solutions were prepared in concentrations of 0.1 and 0.01 M using distilled water. The pH of the exposure solutions was measured prior to introducing the paste specimens using a portable pH meter. In the case of the acetic acid solutions, the initial pH values measured were 2.96 and 3.46 for the 0.1 and 0.01M solutions respectively. Corresponding values of 2.95 and 3.24 were obtained for the butyric acid solutions.

Paste specimens were removed from their cylinders, immediately weighed, and placed into their tank with spacers beneath them to ensure even exposure. Measurements of both pH and specimen mass were taken at intervals throughout the 90-day exposure period.

2.4 Micro-CT scanning

A Nikon XTH225ST micro-CT scanner was used to obtain 3-dimensional images of the interior of the cement paste specimens after exposure to acid. The sample was located 150 mm away from the X-ray source. A tungsten excitation target lens was used, under operating conditions of 115 kV and 312 µA. A 0.5 mm copper filter was used to obtain a suitable image quality. The specimens were revolved in 0.11 ° increments and images were generated using a 2-frame averaging technique at each increment.

2.5 Powder X-ray diffraction

After curing, a specimen from each cement type was crushed and pulverized to a fine powder for analysis using powder X-ray diffraction. The powdered samples were stored overnight in a desiccator containing silica gel and soda lime. Three sub-samples were taken from each powdered sample, with a 5% by mass corundum internal standard added to one. Two of the sub-samples were analysed using a Siemens D5000 powder X-ray diffractometer using a Cu-kα source operating at 40 mA and 40 kV. Scans were obtained using angular increments of 0.1 °2θ at a rate of 0.67 °2θ/minute.

After exposure to the acid solutions, the acid deteriorated layer which had formed around the specimens exposed to the higher concentration solutions was scraped away using a scalpel. This material was pulverized in a pestle and mortar and three sub-samples were taken with two analysed in the same manner as before.

The traces obtained from powder X-ray diffraction were analysed using Rietveld refinement to obtain quantitative estimates of crystalline phases. Rietveld refinement was conducted using the MAUD software package [16]. During refinement, iron was permitted to substitute for aluminium in the structures of the AFm (monosulfate only) and AFt phases, where present.

Using the quantitative determination of the corundum internal standard, it was possible to estimate the quantity of amorphous material present in each sample.

2.6 X-ray fluorescence spectrometry

The remaining sub-samples taken from the acid-deteriorated layers were used to determine their chemical composition using X-ray fluorescence spectrometry. Samples were prepared as pressed pellets which were analysed using a Panalytical Zetium 2.4W X-ray fluorescence spectrometer.

2.7 Geochemical modelling

Geochemical modelling was conducted using the US Geological Service PHREEQC software package [17,18]. The modelling process utilized PHREEQC's TRANSPORT keyword to simulate the movement of acidic species into the pores of a paste specimen via diffusion, and their interaction with cement hydration products at a temperature of 25 °C – using the EQUILIBRIUM_PHASES keyword.

The models consisted of 102 cells linked in sequence. The first of these cells was closed on one end and open to the adjoining cell. It contained 4 kg of water in which the acidic species was dissolved, representing the solution in the exposure tank.

The next cell contained 467 mg of water, a length of 0.1mm, and contained the same concentration of acid. This cell was used as a zone around the surface of the cement paste specimen in which salts could potentially precipitate against the specimen surface [19]. The reason for employing this approach was to differentiate between precipitation of salts some distance away from the specimen surface, and precipitation directly against the surface. The former process would have no impact on the change in mass of the specimen. The latter process could impact on the mass of the specimen – if adhesion between the salt and the surface occurred - and could also impact on mass transport through the degraded surface layer.

The next 100 cells represented the cement paste and its porosity and consisted of 97 mg of pure water in contact with an assemblage of hydration products whose total volume was 370 mm^3 defined using PHREEQC's EQUILIBRIUM_PHASES keyword. Thus, the volume fraction of porosity was initially 0.21.

The last of these cells was closed. This approach introduces a discrepancy with respect to the experimental configuration, since, if the model perfectly resembled the cylindrical specimens used, the volume of material in the cells should decline with depth beneath the surface. This issue does not

make a significant difference to the outcome of the modelling process from a mechanistic perspective, since the excess mass of material that is created by this approach is effectively located at the core of the modelled paste cylinder, and, thus, not involved in the reactions. However, it does potentially mean that the mass transport characteristics used to reproduce the experimental results are overestimates. This does not affect the comparison of these values between cement type.

The composition of the mineral assemblage was obtained by using an optimization process to obtain a mixture of probable cement hydration products which matched the oxide analyses (in terms of CaO, SiO_2, Al_2O_3 and Fe_2O_3) in Table 4, once the contribution from wholly inert constituents (quartz, mullite, hematite, magnetite, perovskite) determined using X-ray diffraction had been subtracted. The results of this process are shown in Table 5. The Ca/Si ratio of the C-S-H phase was permitted to vary between 0.7 and 2.3.

Table 5. Composition of the modelled mineral assemblages within each model cell

	QUANTITY, moles		
PHASE	**PC**	**PC / FA**	**CSA**
Portlandite	2.90×10^{-3}	0.85×10^{-3}	0
C-S-H (Ca/Si = 0.8)	1.03×10^{-3}	1.35×10^{-3}	3.97×10^{-4}
C-S-H (Ca/Si = 1.1)	0	0	0
C-S-H (Ca/Si = 1.8)	0	0	0
Ettringite (Al)	4.52×10^{-9}	1.66×10^{-5}	0.97×10^{-4}
Ettringite (Fe)	0.91×10^{-5}	3.57×10^{-5}	3.30×10^{-5}
Monosulfate (Al)	0.65×10^{-4}	0	0
Monosulfate (Fe)	4.10×10^{-5}	0	0
C_2AH_8	1.26×10^{-4}	3.39×10^{-7}	0.93×10^{-3}
C_2FH_8	2.10×10^{-5}	0.83×10^{-4}	0.74×10^{-5}
C_3AH_6	1.46×10^{-5}	3.05×10^{-4}	0
Gibbsite	0	0	4.86×10^{-4}
Ferrihydrite	0	0	0

The AFm and AFt phases were treated as having both Al and Fe forms, rather than treated as forming solid solutions. The optimization process employed a range of common hydration products, meaning that it was likely that optimization arrived at one of a number of solutions which matched the oxide analysis. Thus, the result of optimization did not necessarily reflect the actual composition of the hydrated cements. However, once assemblage behaviour in contact with water was modelled using PHREEQC, an assemblage which was in equilibrium with its surroundings was obtained, which was presumably more representative of the composition of the actual cement hardened pastes.

The MINTEQ database (version 4) [20] was used as the basic dataset for PHREEQC speciation calculations. To this, data relating to cement hydration products from Lothenbach *et al* [21] was added, plus the data presented in Tables 1-3. C-S-H was included in the model as three individual phases having different Ca/Si ratios (0.8, 1.1 and 1.8), plus silica gel. Solubility products from De Windt and Devillers [22, 23] were used for these phases. The MINTEQ database solubility product for 'amorphous silica gel' ($\log K_{sp} = 2.71$) was used.

It can be seen that the optimization process used to produce a mineral assemblage arrived at a C-S-H phase composition closest to a Ca/Si ratio of 0.8 for all three cements (Table 5). However, the other phases were included in the model at quantities of 0 moles, to permit their precipitation during the modelling process. For the same reason, ferrihydrite ($Fe(OH)_3$) was included in the mineral assemblage at 0 moles, as were any salts formed by the acid being modeled.

The redox potential of the cement pore solutions was set to a pE of 2.54, which is typical of cement where sulfides are not present [24]. The acid solution was given a pE value of 8.45, which is appropriate for water containing dissolved oxygen [25].

The mass transport process selected was wholly diffusion-driven. The models were initially run with an arbitrary diffusion coefficient which was the same for all aqueous species and the change in pH with time of the solution in the exposure tank was compared against the experimental results. The diffusion coefficient was then adjusted until a fit between modelled and experimental results was obtained. Thus, an effective diffusion coefficient for the degraded layer was obtained.

Fitting of modelled results to experimental results was conducted in one of two ways. In some cases - where acid concentrations were low - complete neutralization of the acid was observed. This took the form of a relatively abrupt change from a low to a high pH. Where such an event took place, fitting took the form of adjusting the diffusion coefficient until the pH of the mid-point between the pH values before and after neutralization in the modelled and experimental data occurred within 0.5 of a day of each other.

In other cases, neutralization did not occur. In such cases, the diffusion coefficient was adjusted until the experimental and modelled 90-day pH values were within 0.1 of a pH unit. By employing two different approaches, there exists the potential for the introduction of discrepancies between the diffusion coefficients obtained. However, for a given acid concentration, it is likely that comparison of coefficients between cement types is broadly valid, since the same approach will have been used for at least two of the cements.

Due to the manner in which the models were to be used, no attempt was made to mimic changes in diffusion coefficient resulting from changes in the total volume of the assemblage of phases in each cell during acid attack. Similarly, whilst the experimental results indicated erosion of the outer surface of some specimens, the impact of such a process on mass transfer rates was not addressed.

3. RESULTS

3.1 Mass loss

Figures 1 and 2 show the mass loss for all three cement pastes in acetic and butyric acid solutions respectively. The rate of mass loss from the specimens exposed to the stronger solutions is higher. In the case of the lower concentration solutions, the PC pastes undergo the largest amount of mass loss, followed by the PC/FA pastes.

At the stronger concentration, mass loss is highest for the CSA paste, followed by the PC paste. The mass loss curves obtained from the PC and PC/FA pastes are similar for both acids. However, in the case of the CSA pastes, mass loss is notably higher for exposure to acetic acid compared to butyric acid.

3.2 pH measurements

Figures 3 and 4 show the pH values obtained from the exposure solutions plotted against time, for acetic and butyric acid respectively. The results obtained for the different acids are largely similar. In the case of the results obtained from the low concentration acid solutions in contact with PC pastes the pH undergoes a relatively abrupt transition from a low pH to a higher one. This transition indicates the complete neutralization of acid in the exposure tank by the cement.

Neutralization is also seen in the case of the PC/FA specimens, albeit after a period of some days. This can be ascribed to the lower quantities of dissolvable calcium present in these pastes. However, complete neutralization is delayed to a greater extent in the case of butyric acid, a feature which was considered worthy of further investigation in the geochemical modelling work.

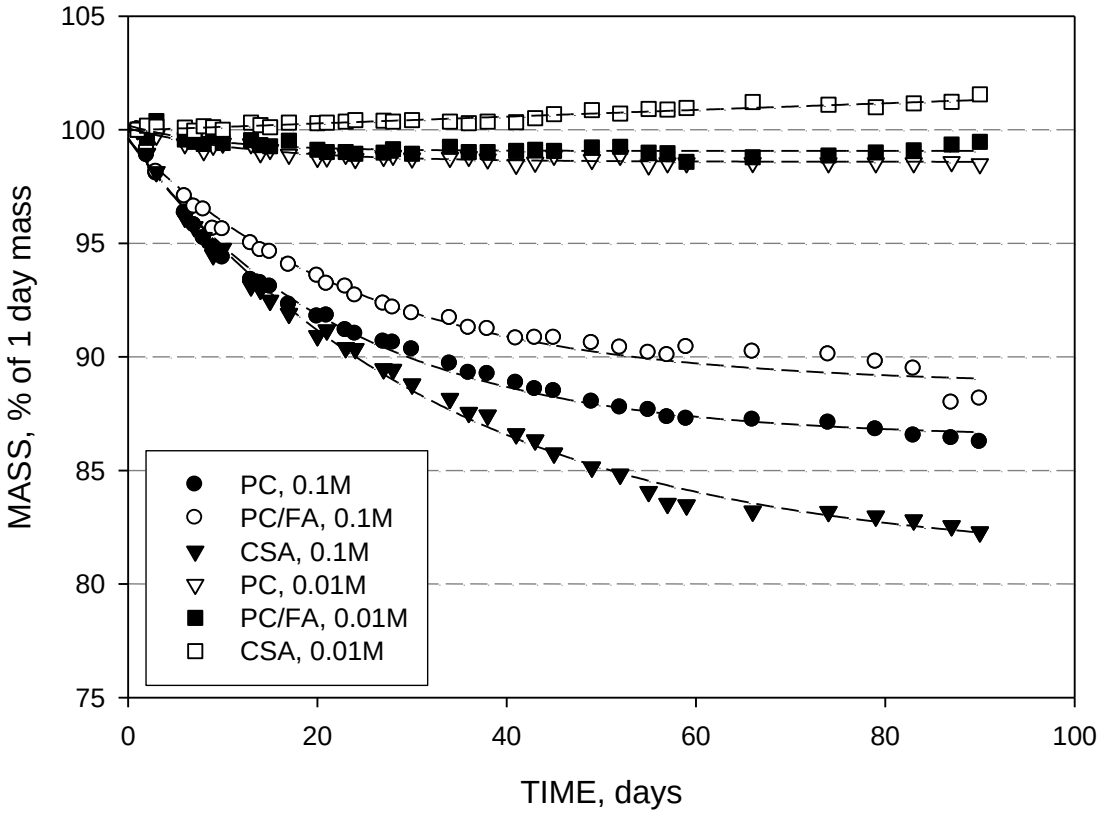

Figure 1. Mass loss from cement paste specimens exposed to acetic acid.

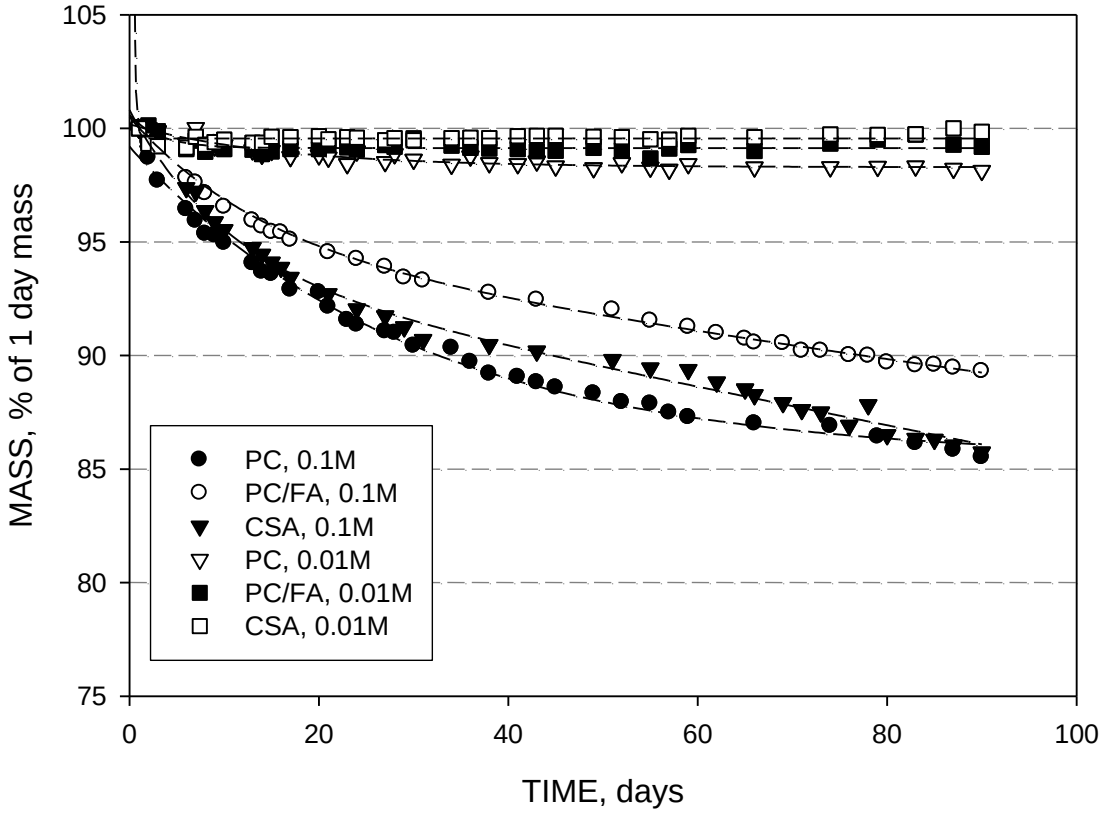

Figure 2. Mass loss from cement paste specimens exposed to butyric acid.

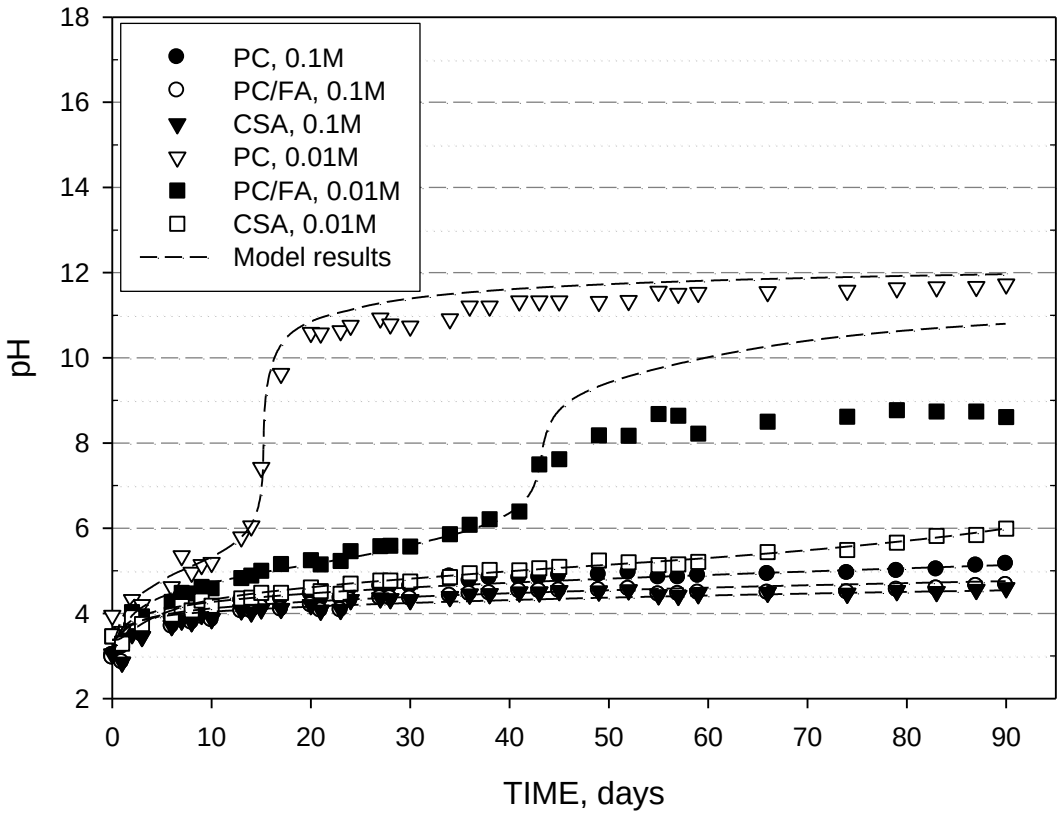

Figure 3. pH of acetic acid solutions in contact with cement paste specimens. Dashed lines show the results obtained using geochemical modelling.

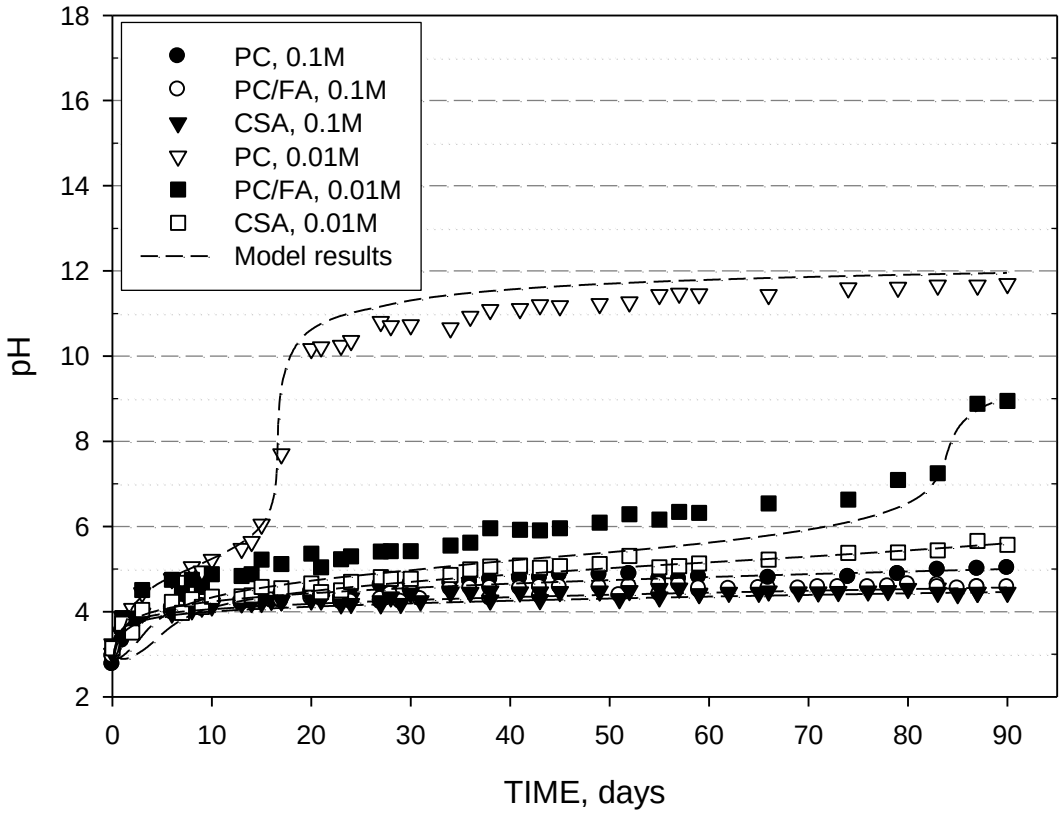

Figure 4. pH of butyric acid solutions in contact with cement paste specimens. Dashed lines show the results obtained using geochemical modelling.

The persistence of acidic conditions in the tanks containing low concentrations of acid and CSA paste specimens was somewhat incongruous in light of the material's high acid neutralization capacity: complete neutralization of the acid solution was not observed. This aspect of performance was also identified as worthy of further examination through geochemical modeling.

In the case of the higher concentration solutions, a low pH was maintained throughout the duration of the experiment.

3.3 Micro-CT scans

Sections through each of the cement paste specimens are shown in Figures 5 and 6. Considerable deterioration of the pastes exposed to the stronger acid solutions has occurred. The nature of deterioration of the PC pastes in high concentration acid solutions follows a pattern which has been observed previously [1], specifically the formation of a completely decalcified layer at the surface of the specimens, followed by a partially-decalcified layer where portlandite is usually absent (which will be referred to as the 'outer core'), and an inner core which is wholly unaffected. The PC/FA and CSA specimens do not possess an outer core, presumably because of the low quantity (in the case of fly ash) or absence (CSA) of portlandite.

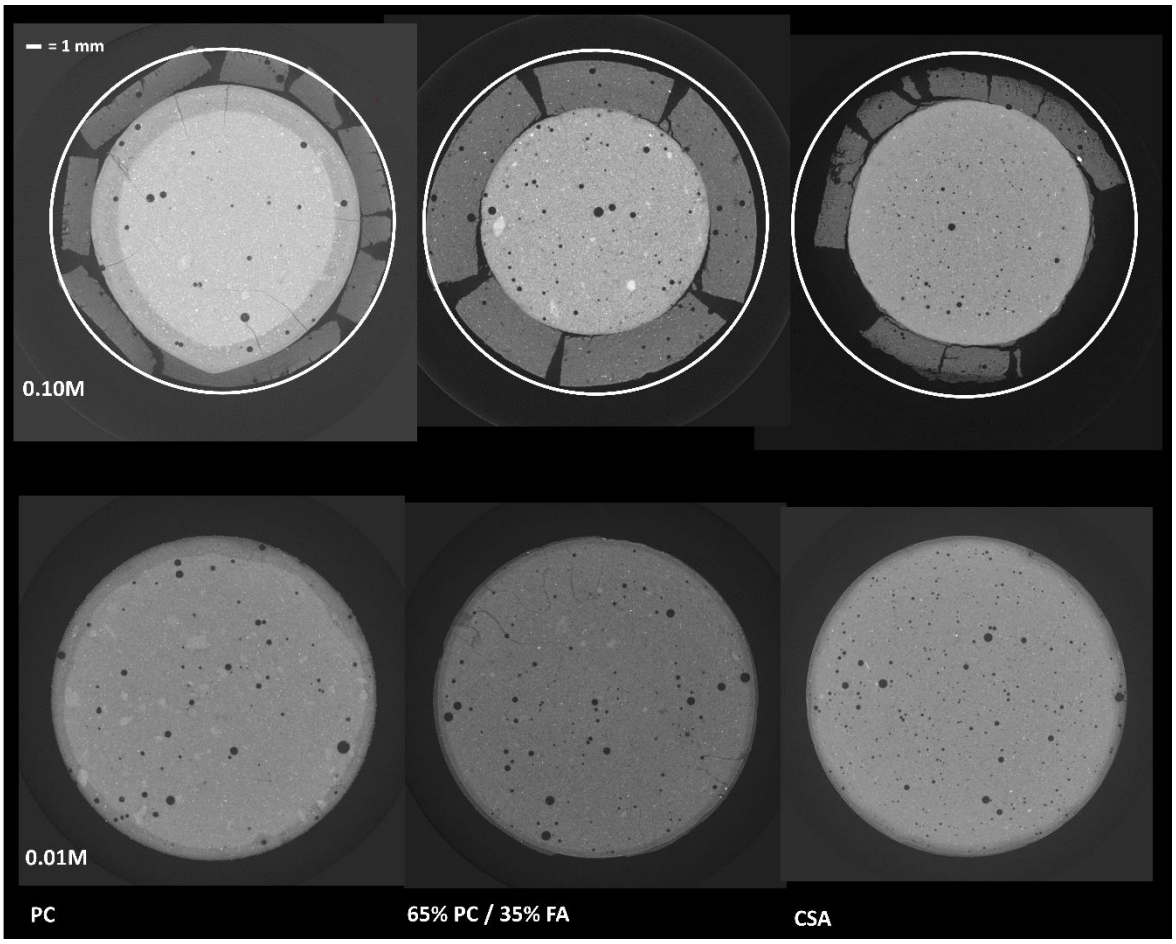

Figure 5. Cross-sections through paste specimens exposed to acetic acid solutions obtained using micro-CT scanning.

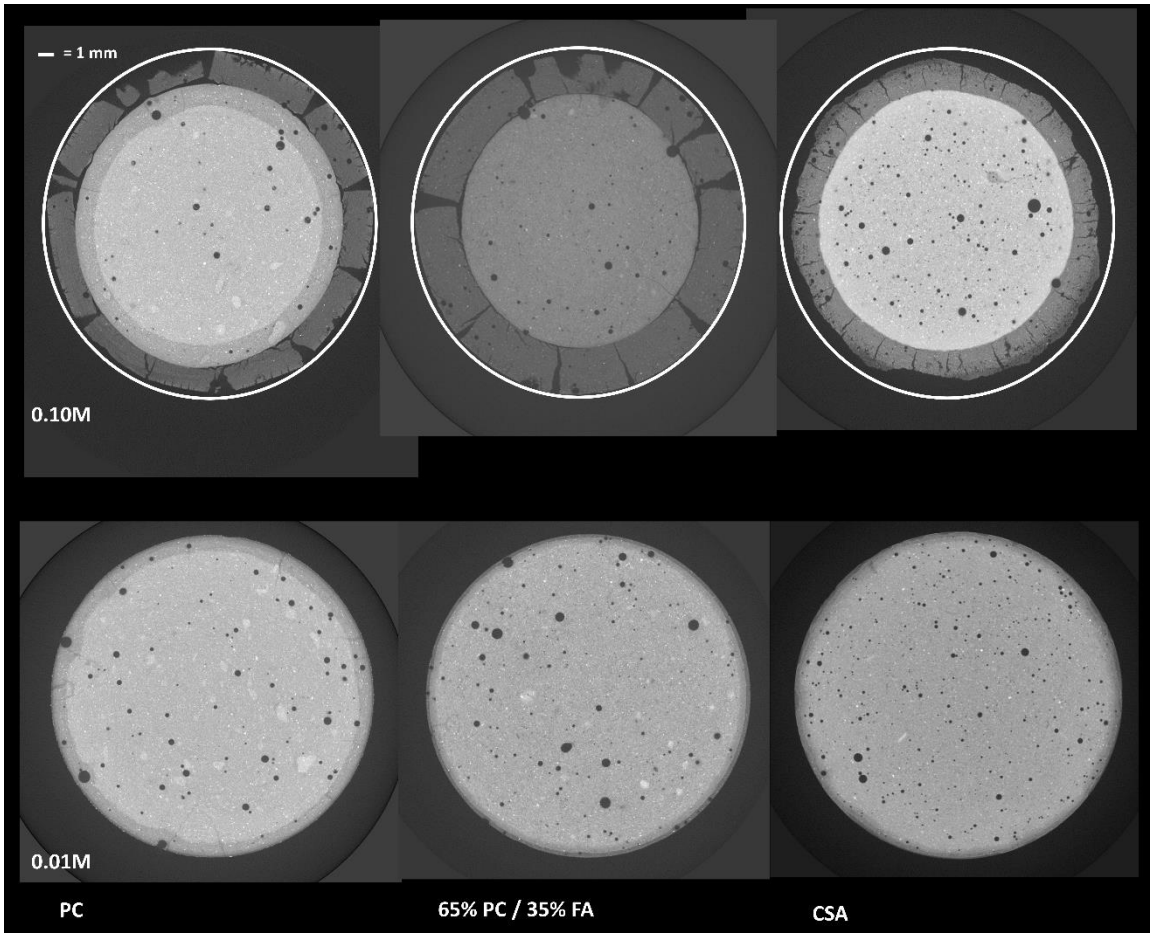

Figure 6. Cross-sections through paste specimens exposed to butyric acid solutions obtained using micro-CT scanning.

In the case of the stronger acid solutions, loss of material at the outer surface is evident, certainly in the case of the CSA specimens. The wholly decalcified layers display significant cracking. However, it should be stressed that cracks were not observed during immersion and only appeared during drying, indicating the high susceptibility of this layer to drying shrinkage. Similarly, the apparent erosion of the surfaces may partly be the result of shrinkage. However, it seems reasonable to assume that the uneven edge of the CSA specimens indicates genuine removal of material. This loss of material from the outer layer was identified as an aspect requiring further investigation using geochemical modeling.

In the case of the low concentration solutions, all three specimens appear to possess a partially decalcified outer core, with no evidence of complete decalcification.

Figure 7 plots cross-sectional areas of the various zones measured from the micro-CT scanning images. There is a correlation between these results and the mass loss results, as long as the implications of the CT results are afforded some consideration. In the case of the weaker acid solutions, we see that the area of the outer core correlates approximately to the loss of mass, as a result of the loss of calcium from this layer. In the case of the stronger solutions, two factors need to be considered – the degree to which the specimens are decalcified, and the extent to which their outer surface has been eroded. Thus, whilst the CSA specimens display decalcification to the lowest extent, they have lost more material from their surface.

The position adopted in this paper is that the most important parameter obtained from the micro-CT images is the cross-sectional area of the inner core. The reason for this has been stated in detail elsewhere [19], but, in summary, the largest loss in strength occurs during the formation of the outer

core due to the dissolution of portlandite, leaving large pores in the remaining C-S-H matrix [2]. Thus, in the context of acid resistance, retention of cross-sectional area of the inner core is of greatest importance. Thus, when comparing the behaviour of different pastes, a larger cross-sectional area of inner core indicates superior performance. With this in mind, for both acids and under both of the concentrations studied, the CSA cement paste performs better than the PC/FA, which, in turn, offers greater acid resistance than the PC paste. CSA also appears to be more resistant to butyric acid compared to acetic acid.

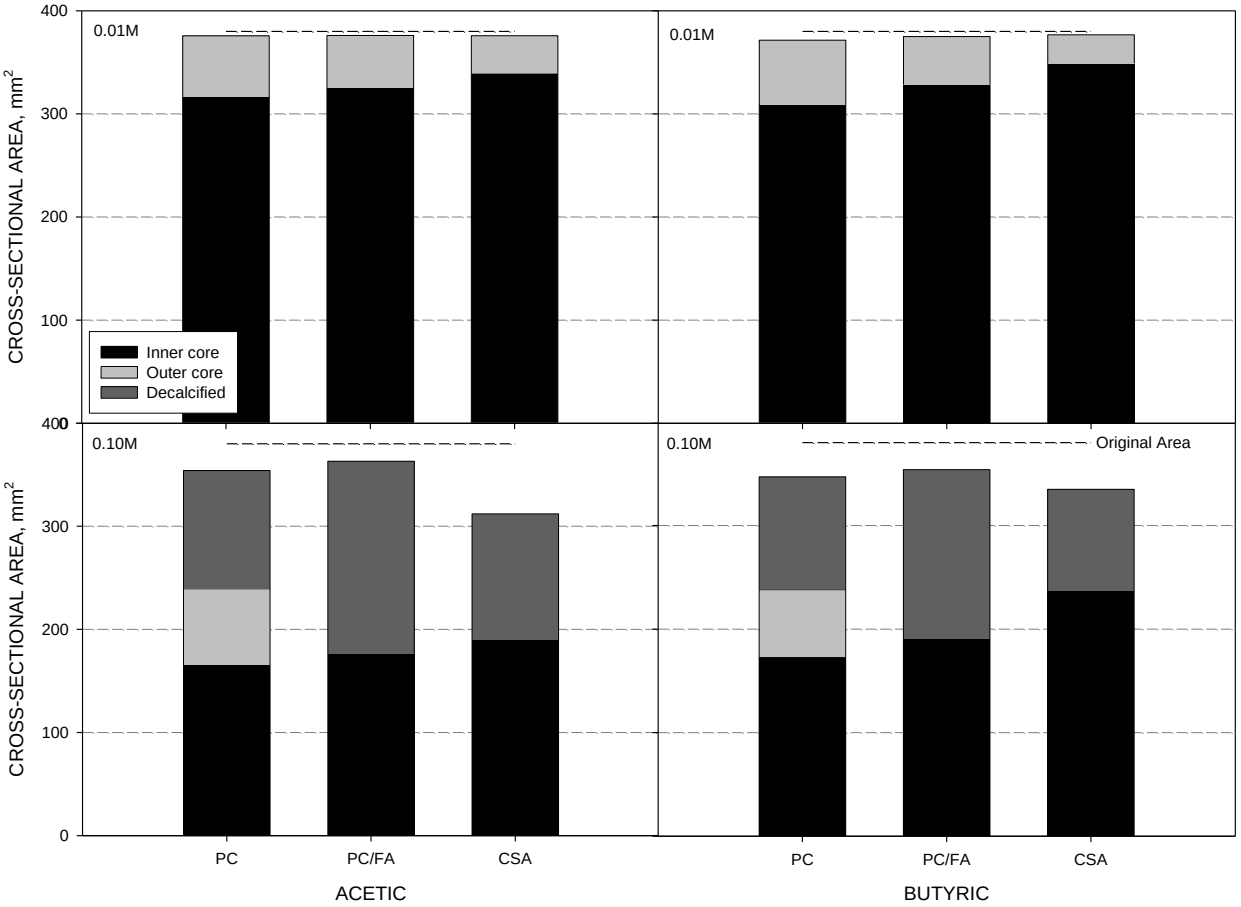

Figure 7. Cross-sectional areas of zones in various states of degradation around cement paste specimens exposed to acid solutions, determined from analysis of micro-CT images.

3.4 Chemical and mineralogical analysis of degraded layers

Table 6 shows the results of XRF analysis of the degraded layers of the paste specimens. It should be noted that these samples solely consisted of wholly decalcified material, and that none of the partially decalcified zone was included. Comparing these compositions against those of the original materials in Table 4, there have been substantial losses with respect to calcium and sulfate as a result of exposure to the acids. One of the main reasons for the better performance of the CSA paste specimens is thus evident: the calcium content of this cement was initially lower, and so loss of dissolvable calcium is limited. Aluminium, silicon and iron are notable in their evident retention in the layer. The sum of these analyses falls short of 100. This is the result of the presence of chemically-bound water, plus elements not covered by the analysis.

Table 6. Results of XRF analysis of the degraded layers taken from the paste specimens.

	%, by mass					
	Acetic			Butyric		
	PC	PC/FA	CSA	PC	PC/FA	CSA
CaO	7.93	4.61	4.28	8.82	4.95	5.12
SiO_2	56.95	55.47	16.81	55.52	54.61	13.72
Al_2O_3	14.06	19.10	46.33	13.68	18.94	46.82
Fe_2O_3	8.34	9.21	4.57	8.11	8.84	5.21
MgO	0.94	1.02	1.00	0.92	1.02	0.97
Na_2O	0.05	0.27	0.02	0.06	0.24	-
K_2O	0.40	1.19	0.05	0.40	1.14	0.05
TiO_2	0.69	1.08	2.97	0.67	1.08	3.94
MnO	0.15	0.08	0.03	0.13	0.09	0.04
P_2O_5	1.39	1.14	0.27	1.45	1.25	0.42
SO_3	0.237	0.161	3.459	0.274	0.196	2.877
Cl	-	0.012	0.015	0.018	0.012	0.015
TOTAL	**91.13**	**93.33**	**79.79**	**90.05**	**92.36**	**79.18**

These results are reflected in the estimated mineralogical compositions of the layers obtained from X-ray diffraction (Table 7). The X-ray diffraction traces obtained from the layers are shown in Figure 8.

Portlandite is entirely absent after exposure to the acids, as are other hydrates. In the case of the PC and PC/FA pastes, the amorphous content of the materials increases, indicating the persistence of decalcified C-S-H phases. Additionally, whilst residual quantities of unreacted C_3S and C_2S in these pastes before exposure to acid are absent after exposure, a persistence of unreacted C_4A_F (which was present in quantities too small to be detected in the original pastes) is evident.

In the case of the CSA pastes, the amorphous content decreases, with a substantial quantity of gibbsite forming from the decomposition of ettringite and strätlingite (and possibly amorphous phases containing aluminium), as discussed previously.

The chemical and mineralogical compositions were used to estimate the composition of the amorphous fraction of each of the pastes both before and after exposure to the acid solutions. Figure 9 shows the change in the chemical composition of the cement pastes after exposure with respect to CaO, SiO_2 and Al_2O_3 in the form of arrows plotted on ternary diagrams. It should be noted that the straight paths described by these arrows across the diagram do not reflect the actual change in composition with respect to time, which would not follow a linear route.

The figure also includes a similar plot for the total chemical composition of the ashes (i.e. including both amorphous and crystalline constituents). Both ternary diagrams resemble each other to a large extent, with the arrows indicating a shift in composition away from CaO and towards SiO_2, as would be expected. The majority of Al_2O_3 is also retained in both the amorphous fraction and the paste as a whole. This is indicated by arrows which can approximately be extrapolated back to the CaO corner of the diagrams. It is worth noting that the only instance where extrapolation yields a significant deviation away from this point is the amorphous fraction of the CSA cement pastes, which reflects the transformation of amorphous Al_2O_3 to more crystalline gibbsite.

With respect to the type of acid the pastes were exposed to, there is, again, very little difference in the alteration of chemical composition in the degraded layer.

Table 7. Results of estimation of mineralogical analysis of the degraded layers taken from the paste specimens, conducted using Rietveld refinement of powder X-ray diffraction traces.

		EXPOSURE								
		Whole specimen, before exposure			Acetic			Butyric		
PHASE	**FORMULA**	**PC**	**PC/FA**	**CSA**	**PC**	**PC/FA**	**CSA**	**PC**	**PC/FA**	**CSA**
Portlandite	$Ca(OH)_2$	10.2	6.0	-	-	-	-	-	-	-
C_3S	Ca_3SiO_5	1.7	0.8	-	-	-	-	-	-	-
C_2S	Ca_2SiO_4	4.2	2.1	3.5	-	-	-	-	-	-
C_3A	$Ca_3Al_2O_6$	-	-	0.6	-	-	-	-	-	-
C_4AF	$Ca_2(Al,Fe)_2O_5$	-	-	-	1.7	1.0	-	2.5	0.7	-
Ye'elimite	$Ca_4Al_6SO_{16}$	-	-	0.4	-	-	-	-	-	-
Ettringite	$Ca_6Al_2(SO_4)_3(OH)_{12}\cdot 26H_2O$	1.8	1.6	3.1	-	-	-	-	-	-
Strätlingite	$Ca_2Al_2(SiO_2)(OH)_{10}\cdot 2.5H_2O$	-	-	7.6	-	-	-	-	-	-
Quartz	SiO_2	-	1.1	-	1.5	6.1	-	1.4	2.5	-
Mullite	$Al_6Si_2O_{13}$	-	1.4	-	-	6.7	-	-	3.9	-
Hematite	Fe_2O_3	-	-	-	-	0.4	-	-	0.2	-
Magnetite	Fe_3O_4	-	0.1	-	-	0.6	-	-	0.3	-
Calcite	$CaCO_3$	-	1.7	-	-	-	-	-	-	-
Gibbsite	$Al(OH)_3$	-	-	0.9	-	-	24.4	-	-	35.7
Perovskite	$CaTiO_3$	-	-	1.0	-	-	2.4	-	-	4.2
Gehlenite	$Ca_2Al(AlSiO_7)$	-	-	4.2	-	-	1.0	-	-	0.1
Monocarbonate	$Ca_4Al_2(CO_3)(OH)_{12}\cdot 5H_2O$	0.3	1.3	-	-	-	-	-	-	-
Monosulfate	$Ca_4Al_2(SO_4)(OH)_{12}\cdot 6H_2O$	0.6	8.2	-	-	-	-	-	-	-
Amorphous	-	77.4	83.5	70.5	96.8	85.2	72.2	96.1	92.3	60.0

3.5 Geochemical modelling

Adequate fits of pH change were obtained for the low concentration acetic acid solutions with diffusion coefficients of 2.30×10^{-13}, 1.70×10^{-13} and 8.50×10^{-14} m^2/s for the PC, PC/FA and CSA pastes respectively. In the case of butyric acid, these values were 2.50×10^{-13}, 1.10×10^{-13} and 9.00×10^{-14} m^2/s. Adequate correlation between the modelled and experimental pH changes for the higher concentration acetic acid solution was obtained with diffusion coefficients of 1.30×10^{-12}, 1.20×10^{-12} and 1.00×10^{-12} m^2/s for PC, PC/FA and CSA pastes respectively. The corresponding values for butyric acid were 9.00×10^{-13}, 8.50×10^{-13} and 6.00×10^{-13} m^2/s. The pH curves obtained by modelling are shown in Figures 3 and 4, alongside the experimental results. Whilst the criteria for obtaining a fit with the experimental data were satisfied in all cases, it is evident that in the case of the PC/FA pastes with low acid concentration the pH values either before or after neutralization of the acid do not fit particularly well with the experimental results. This is most probably due to a proportion of the constituents of the fly ash having not yet undergone pozzolanic reaction, or being wholly unavailable for such reactions. As a result, these constituents do not undergo reaction with the acid.

It should be stressed that the diffusion coefficients are apparent diffusion coefficients, since the value will reflect both the diffusion rate through the unaffected cement paste, as well as, to a much lesser extent, the decalcified zones. Thus, the higher acid concentrations yield higher diffusion coefficients, since these lead to the formation of a fully decalcified zone, which will be more porous.

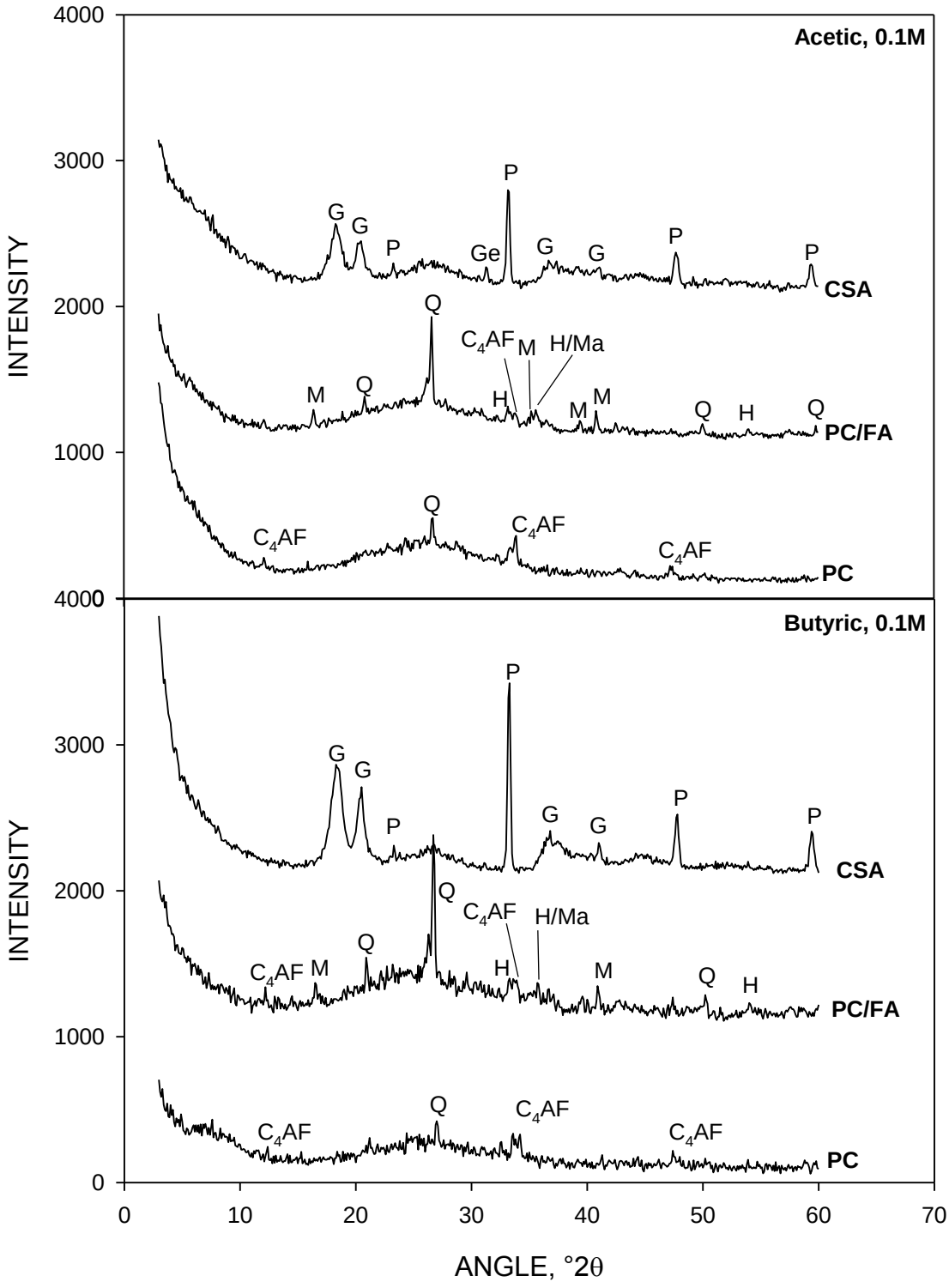

Figure 8. X-ray powder diffraction traces from the degraded layers of cement paste specimens exposed to acid solutions. G = gibbsite; P = perovskite; Ge = gehlenite; M = mullite; Q = quartz; H = hematite; C4AF = tetracalcium aluminoferrite; Ma = magnetite.

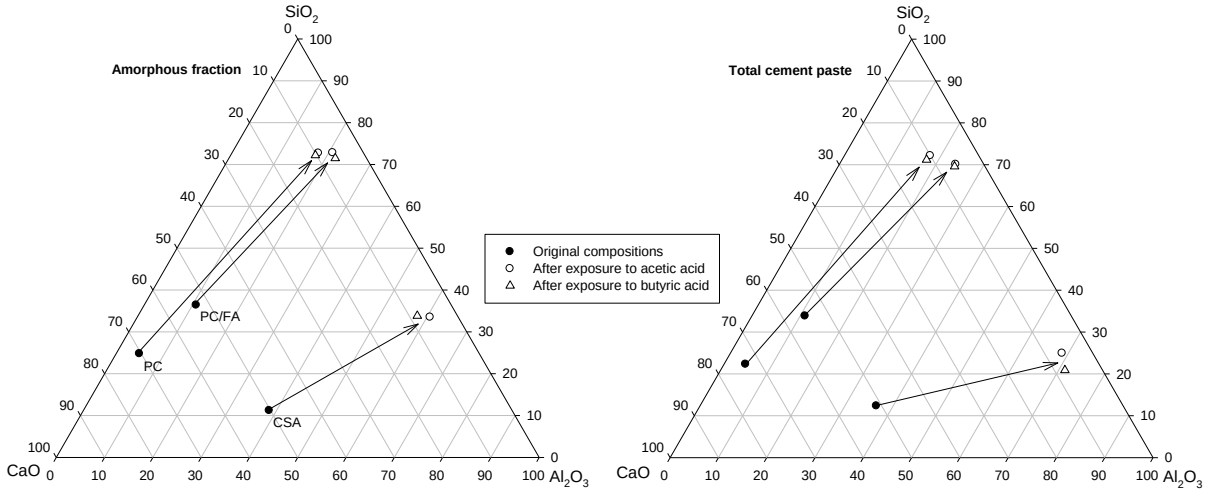

Figure 9. Change in composition of the degraded layer of cement pastes exposed to acetic and butyric acid both in terms of the amorphous fraction and the total mass of cement paste.

3.5.1 PC

Figure 10 shows the mineral compositions of the pastes exposed to a 0.1 M solution of acetic acid after a modelled exposure period of 90 days. In the case of the PC paste, partial decalcification of C-S-H phases is evident, with a shift towards C-S-H phases with progressively lower calcium content, ultimately to the point where only a layer of wholly decalcified silica gel remains at the surface. There are also quantities of gibbsite and ferrihydrite ($Fe(OH)_3$). These phases were not identified by X-ray diffraction, but the quantities of Al_2O_3 and Fe_2O_3 evident in the degraded layers indicate that iron and aluminium are retained in this zone. This is because the pH at the specimen surface is insufficiently low to allow dissolution of gibbsite and ferrihydrite, leading to an accumulation of these phases [26]. These hydroxide phases are presumably present as amorphous forms, since their presence was not evident in the X-ray diffraction traces – other than gibbsite in the CSA pastes. The results for butyric acid were similar to those for acetic acid.

Whilst the low-solubility aluminium diacetate and iron (III) diacetate phases were included in the model as compounds whose precipitation was possible, these phase were not formed in any of the modelled pastes. The reason for this is simply that gibbsite and ferrihydrite are considerably less soluble, and so were precipitated instead.

3.5.2 PC/FA

Figure 10 also shows the same results for the PC/FA paste. Whilst the results are generally similar to the PC results, it is evident that there is a complete absence of portlandite in the unaffected paste. This is the result of the geochemical modelling process establishing an equilibrium, which is not reflected in the real specimens. It is likely that the real specimens would approach the mineralogical composition predicted by the model if and once complete reaction of the fly ash particles was complete. It is likely that further progression of this reaction would have occurred during exposure to the acid solution.

Modelled exposure clearly yields a partially decalcified zone in the PC/FA paste. Such a zone was not evident on the CT scans. However, the drop in calcium content across this zone is less for the PC/FA paste in comparison to the PC paste, which is most probably the reason for its apparent absence in the CT images.

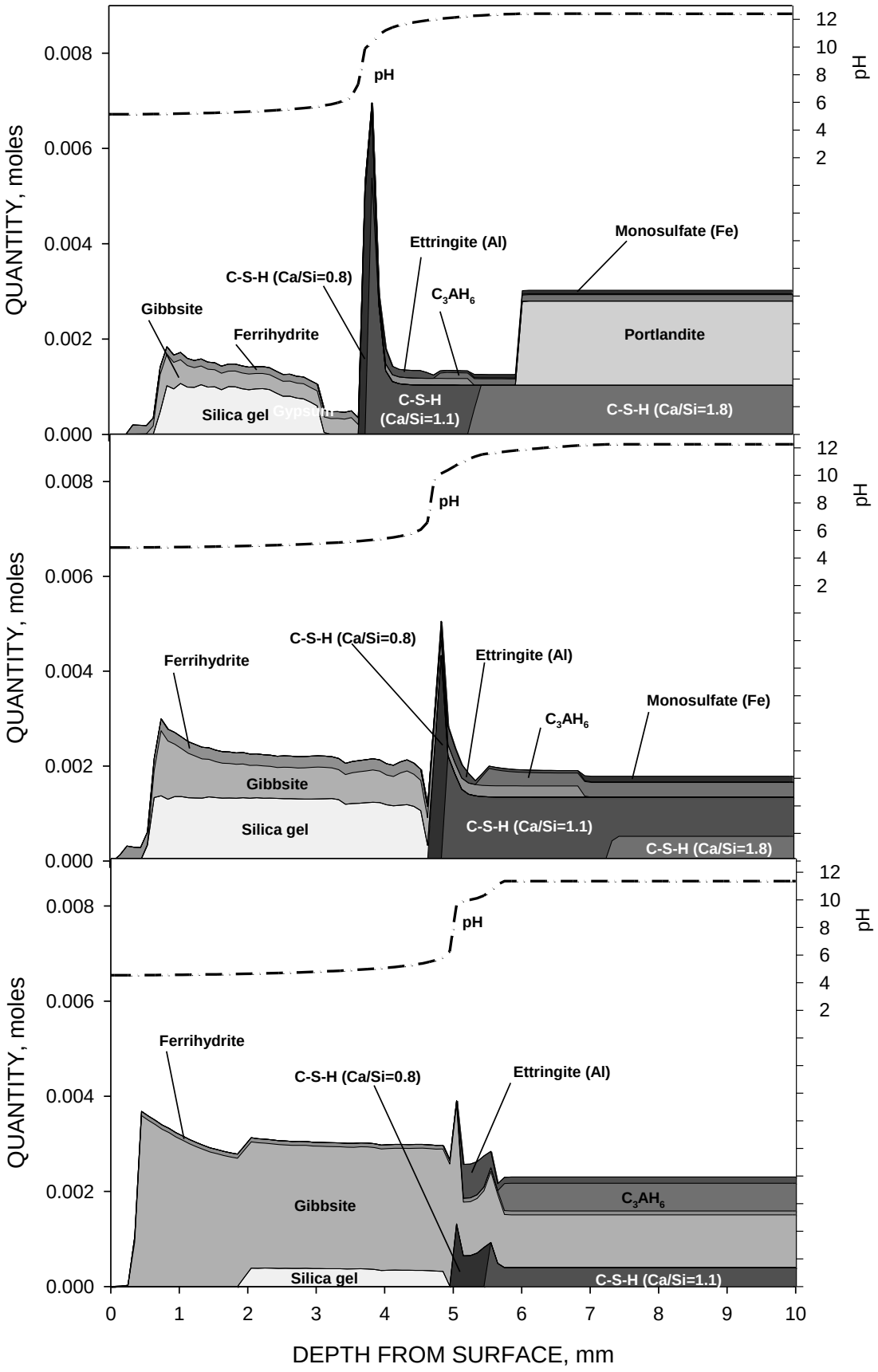

Figure 10. Results of geochemical modelling: solid phases present in the modelled paste specimens exposed to a 0.1M acetic acid solution for 90 days.

In the case of both acids, most of the complexes formed between metal ions in the cements were weak. However, in the case of acetic acid, slightly stronger complexes are formed with iron (III). The PC/FA paste had the highest iron content, and so examination of this aspect is of most relevance for this material. Examination of the model output indicated that all three acetate-iron (III) complexes became evident at pH conditions of less than 7 (i.e. close to the surface of the specimen), with the 1:3 complex being dominant. The concentration of dissolved iron in the modelled PC/FA paste exposed to 0.1M acetic acid close to the surface was around three times that in the paste exposed to the same concentration of butyric acid, where complexes were not formed.

The overall effect of complexation, however, is minor, with the modeled concentration of dissolved iron in the paste exposed to the 0.1M acetic acid solution only reaching a concentration of around 0.04 mol/l. This is reflected in the levels of ferrihydrite present in the modelled results, which do not show signs of notable dissolution of ferrihydrite close to the surface. This is also seen in the experimental results in Table 6, where there is very little difference in the quantities of iron present in the degraded layers of the specimens regardless of whether they were exposed to acetic or butyric acid (whose iron complexes are presumably weak).

3.5.3 CSA

The mineral composition resulting from geochemical modelling of 0.1M acetic acid exposure for the CSA paste indicates the formation of additional gibbsite in the decalcified zone, reflecting the X-ray diffraction results in Table 7. Thus, the modelled cement has undergone the first stage of acid attack of calcium aluminate cement discussed in the introduction (the decomposition of calcium aluminate hydrates), but the second stage (amphoteric dissolution of $Al(OH)_3$) has occurred to a lesser extent.

It should be noted that, notwithstanding the above discussion, the outermost surfaces of all the modeled pastes *did* – to varying degrees - dissolve. Whilst the pH conditions at these locations do not favour the dissolution of phases such as gibbsite and silica gel, dissolution on a small scale still occurs. The dissolved species diffuse either out into the exposure solution or further into the paste - where the higher pH causes their re-precipitation. This migration allows further dissolution, eventually causing complete dissolution to a certain depth. The re-precipitation of gibbsite in the model leads to a peak in gibbsite close to the surface of the pastes.

The loss of material from the outer surface of the CSA specimens observed in the experiments was not evident to the same extent in the model results shown in Figure 10. However, what is evident is the complete dissolution of silica gel to a certain depth at the surface. This suggests that the silica gel in the degraded layer of the CSA pastes acts as a means of maintaining physical attachment of gibbsite at the specimen surface, since the depth to which silica gel is absent approximately matches the depth of complete material loss from the outside of the CSA specimen in the experiments. This is conceivable, since the re-precipitation of gibbsite described in the introduction requires a surface on which it can be deposited if it is to remain part of the specimen. Clearly, the dissolution of all solid phases including silica gel removes such surfaces from the outermost region of the paste. This would mean that gibbsite will either be deposited as discrete particles a distance away from the paste, or remain dissolved in the large volume of water in the exposure tank. Fine particles on the tank bottom were observed during the experiments. This process was not dealt with by the model, and so a discrepancy exists here between experimental and modelled results in this respect.

The unrealized neutralization capacity of the CSA cement is illustrated further in Figures 11 and 12, where the quantity of phases involved in acid attack are plotted against time for the models of the PC and CSA pastes exposed to the 0.1 M acetic acid solution. In the case of the PC paste, the largest change is the decrease in the quantity of portlandite, although there is also a decline in the quantity of C-S-H with a Ca/Si ratio of 1.8 (replaced with a C-S-H phase with a lower Ca/Si ratio) and iron monosulfate.

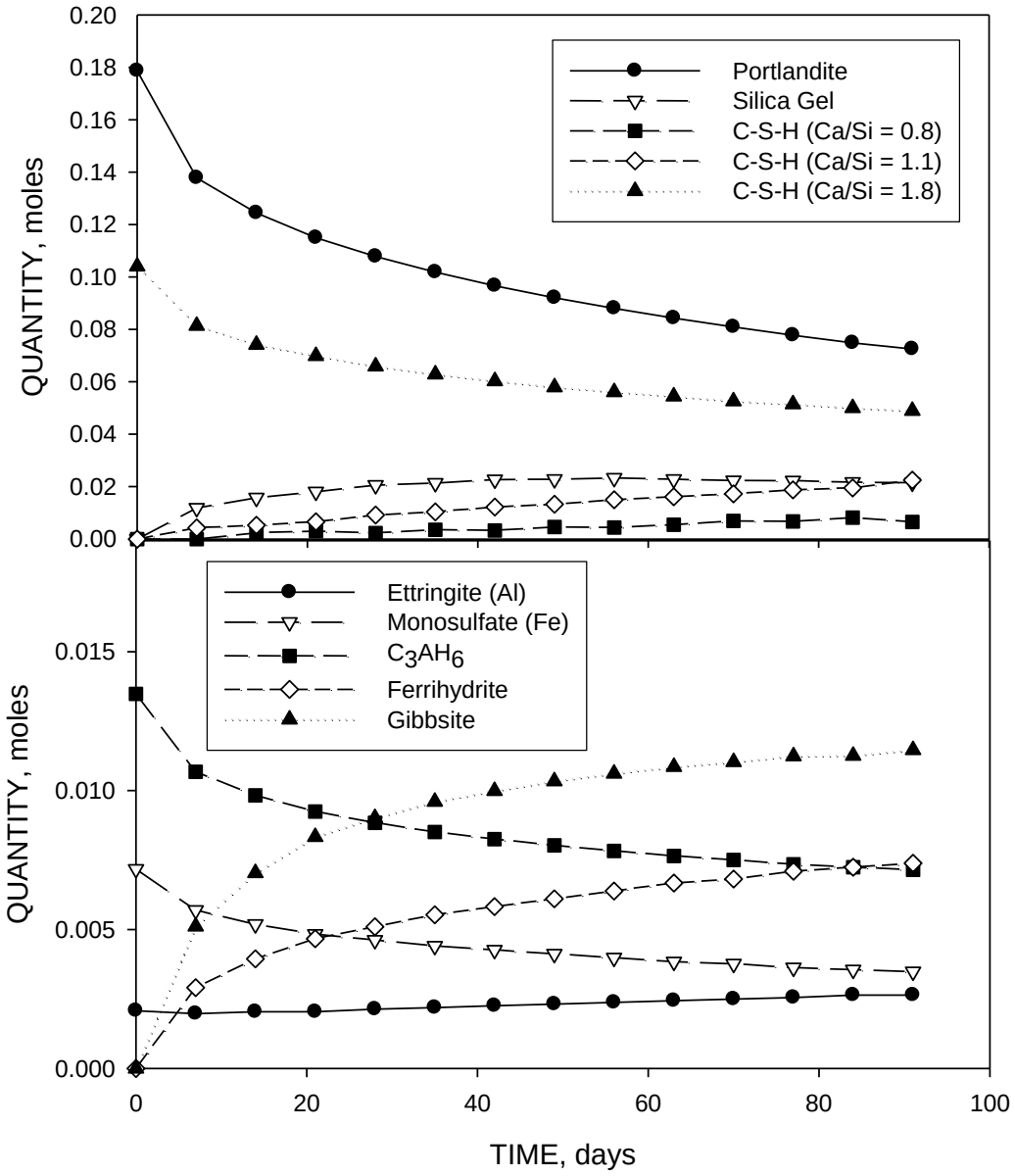

Figure 11. Results of geochemical modelling: quantities of hydration products in the entire PC paste specimen exposed to 0.1M acetic acid versus time.

In the case of the CSA paste, whilst there is a decline in the quantities of C_3AH_6 and C-S-H phases, there is an increase in gibbsite, due to the dissolution of calcium aluminate hydrate phases and the re-precipitation of aluminium as hydroxide. This is not to say that gibbsite is not contributing towards neutralization in any way – it is evident that a quantity of the phase will partially dissolve from outer parts of the paste where the pH is sufficiently low. However, the absence of calcium aluminate hydrate phases and the re-precipitation and accumulation of gibbsite indicates that the first stage of the reaction between hardened CSA cement paste described in the introduction has occurred to a much greater extent than the second.

This explains why neutralization of the acids in Figures 3 and 4 was not observed in the case of the experiments where CSA cement paste specimens were exposed to 0.01M acid solutions. This presents an interesting feature of the acid neutralization reactions of calcium aluminate cements – where low acid concentrations or acids with high pKa values are involved, there exists the possibility that the low pH conditions needed to realise the full acid neutralization capacity might not be encountered. Thus,

the period of time required for neutralization will be protracted. During this time, diffusion of acidic species into the cement will continue, with subsequent growth of the depth of the deteriorated layer. In such cases, greater resistance in the form of improved acid neutralization capacity is likely to be offset to some extent by the slower progress of neutralization.

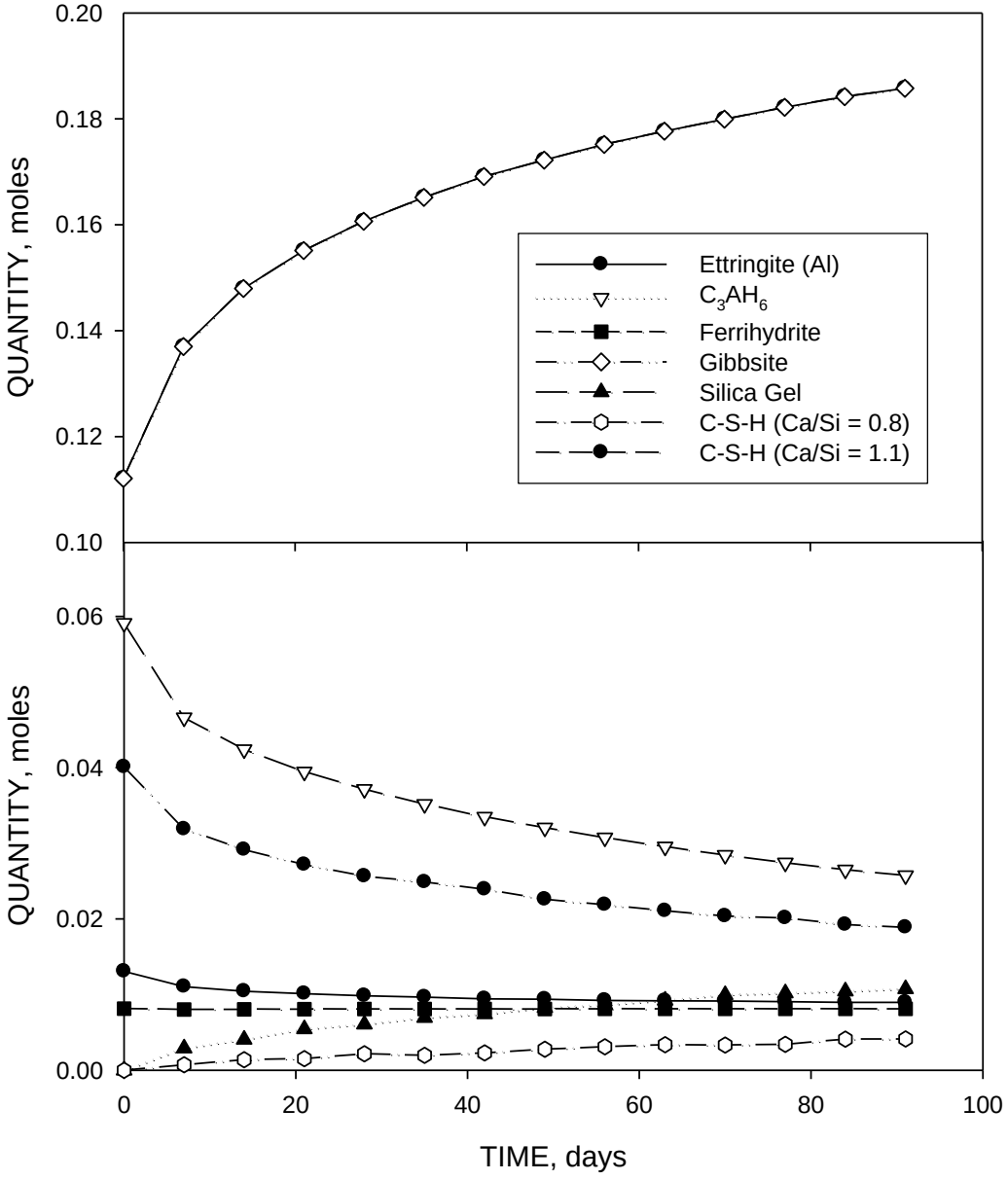

Figure 12. Results of geochemical modelling: quantities of hydration products in the entire CSA paste specimen exposed to 0.1M acetic acid versus time.

This effect has been observed experimentally in previous research examining the exposure of hardened calcium aluminate cement paste to the very weak acid, catechol [19]. The development of a deteriorated layer progresses at a rate comparable to that of much stronger acids (such as tartaric acid). However, the remaining gibbsite in the deteriorated layer dissolves negligibly, meaning that the original shape of the paste specimen is maintained. Thus, unlike in the case of stronger acids, no advantage in performance is observed in the case of the CSA paste when compared to a PC paste where catechol is the attacking acid.

This effect was explored further, again using geochemical modelling. Figure 13 shows the development of decalcified and partially decalcified zones in the cement pastes during modelled exposure to a notional monoprotic acid of varying pK_a for 90 days, assuming a constant diffusion coefficient for all materials. The acid was assumed to form no complexes with metal ions. Additionally, the interpretation of the PC/FA results assumed that the partially decalcified zone observed in the model was sufficiently similar to the inner core to be classed as such, as appears to be the case from the CT scans.

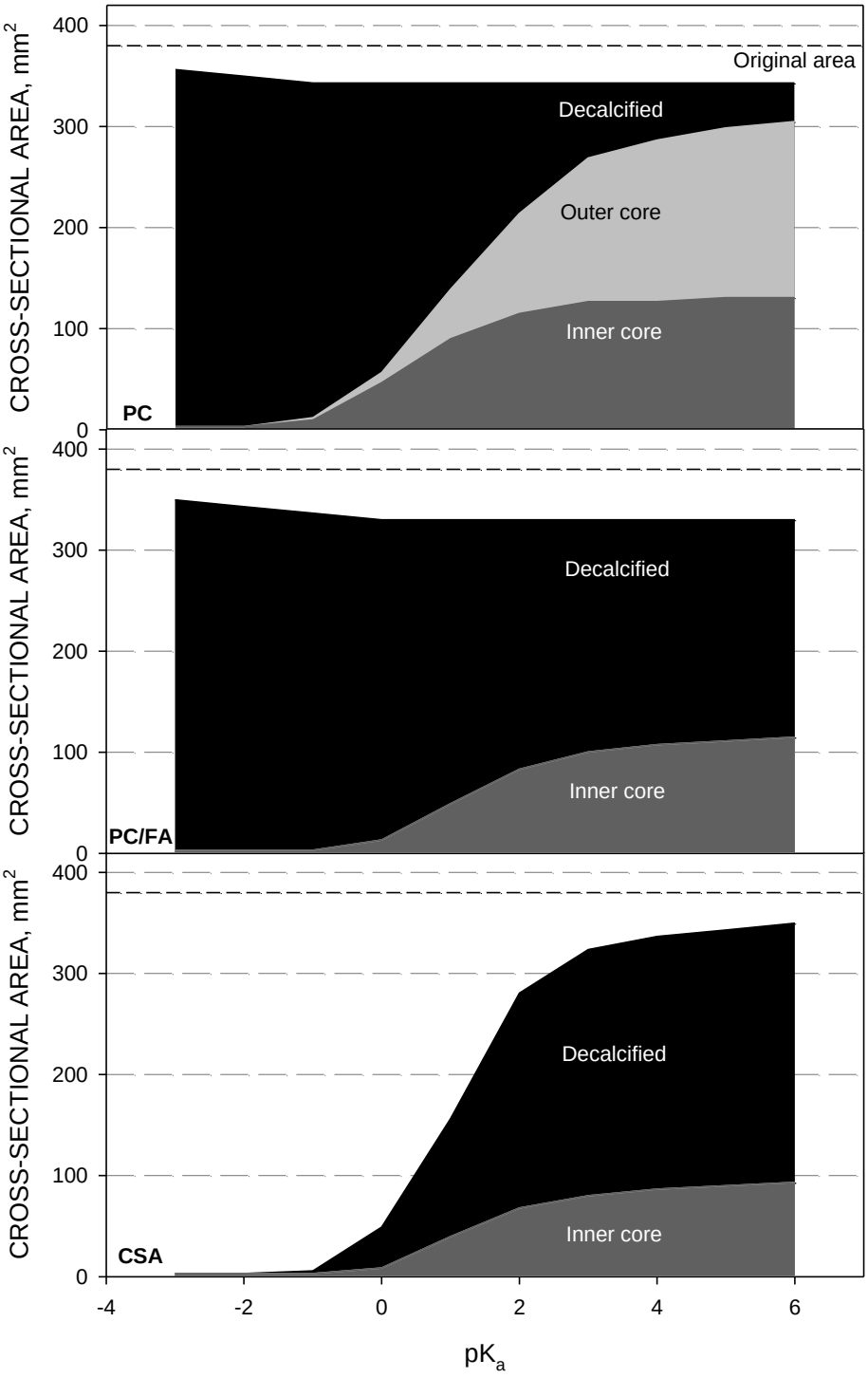

Figure 13. Results of geochemical modelling: cross-sectional areas of zones in various states of deterioration around cement paste specimens exposed to a 0.1M solution of a notional acid of varying pKa. A diffusion coefficient of 1.3×10^{-12} m^2/s has been used throughout.

At high pK_a values (and, hence, at low acidic strength) the depth of deterioration in terms of the cross-sectional area of the inner core of cement paste remains constant from the upper pK_a considered – 6 - down to around 2, although the remaining inner core is slightly smaller for the PC/FA and CSA pastes. As acid strength increases, the depth of deterioration increases. As pK_a decreases further, the difference between the materials reduces. Also of note is the loss of decalcified material at the outer surface of the CSA specimen as pK_a decreases, in contrast to the persistence of a decalcified layer in the PC specimen. This is because lower pK_a values will yield lower pH values for a given concentration of acid, causing gibbsite to dissolve.

The significance of these results requires some discussion. Whilst some caution must always be exercised when using modelled results to interpret experimental results, the model used to generate the results presented in Figure 13 relies predominantly on established chemical characteristics – specifically pKa and the solubility behaviour of the cement hydration products. By using the same diffusion coefficient throughout, it is the chemical behaviour of the cements and the notional acid which are under investigation.

When the pKa of the acid is higher (as is the case for acetic and butyric acid), the ability of the different cement types at resisting acid attack in the model is the opposite of the behaviour observed experimentally. Thus, where pKa is high, PC pastes are better able to resist acid attack through chemical means than PC/FA and CSA pastes.

It must be stressed that the CSA paste in these experiments still clearly outperforms the PC and PC/FA pastes. It can therefore be supposed that, in the experiments, the diffusion coefficients of the acids through the degraded layer were very different for the different cement types, and followed the sequence PC > PC/FA > CSA. This was, indeed, what was seen when the model data was fit to the experimental results.

The reasons for the lower diffusion coefficients across the degraded layers of the PC/FA and CSA pastes can be attributed to two factors. Firstly, this may in part be the result of differences in the particle size distribution of the original cements and the nature of the original hydration products from these cements. Whilst the microstructure of the pastes in the degraded zone will have been altered significantly by exposure to acid, the residual porosity characteristics of the pastes will still have an influence. Secondly, the dissolution and re-precipitation of gibbsite in the degraded zone will have the effect of depositing solid material onto the surface of pores, reducing the volume of porosity and pore diameters. As discussed previously, this re-precipitation in the decalcified zone is likely to occur in pores, thus reducing both pore size and volume and limiting rates of mass transport [3]. This effect will be more pronounced in the PC/FA and, especially, the CSA pastes, where the aluminium content of the cements is higher.

The behaviour described in Figure 13 is clearly dependent on the specific exposure conditions: with higher acid concentrations yielding lower pH conditions for an acid of a given strength, leading to greater depths of deterioration after a given time. Additionally, multi-protic acids will give greater depths of deterioration.

4. CONCLUSIONS

This paper has reported on the evaluation of the performance of three types of cement paste (PC, PC/FA and CSA) using both laboratory experiments and geochemical modelling. The most significant observations are summarized below.

- The similarity between the acid dissociation constants of acetic and butyric acid means that the general behaviour of cements exposed to these substances was also similar. This took the

form of the partial decalcification of C-S-H in the case of lower acid concentrations, and the formation of a wholly decalcified layers at higher concentrations.

- Whilst the decalcified zone of the PC and PC/FA cement pastes consists of silica gel, in the case of CSA it consists of an aluminium-rich material containing significant quantities of gibbsite.
- Mass loss from CSA specimens was greater than for the other cement types. However, this does not reflect a greater rate of deterioration. Instead it reflects the removal of material from the outer surface of the decalcified zone, which did not occur for the pastes containing PC.
- Whilst calcium aluminate cements have a higher acid neutralization capacity than Portland cement, the experimental results and the results of geochemical modelling show that exposure to low concentration acid solutions or weak acids will lead to only partial neutralization, causing the full neutralization capacity to remain unrealized and allowing deterioration to proceed. This is the result of the pH in such circumstances being insufficiently low to dissolve gibbsite which has been precipitated as a result of reactions between the acid and calcium aluminate cement hydration products.
- Despite this, the CSA cement outperformed the PC paste specimen with regards to acid resistance. The paste containing FA performed less well in comparison to CSA, but was more acid resistance than the PC paste. The superior performance of CSA is, thus, most likely to be the result of improved microstructural characteristics, and a consequent reduced rate of diffusion. The enhanced performance of FA is most probably the result of the low portlandite content of this paste.

5. ACKNOWLEDGEMENTS

The author would like to thank Mr Andrew Forsyth for assistance with the experimental work reported in this paper. The author also wishes to acknowledge the use of the EPSRC-funded National Chemical Database Service hosted by the Royal Society of Chemistry.

6. REFERENCES

1. A. Bertron and J. Duchesne, Attack of cementitious materials by organic acids in agricultural and agrofood effluents, in: M. Alexander, N. De Belie and A. Bertron (Eds.), Performance of Cement - based Materials in Aggressive Aqueous Environments, RILEM State - of - the - Art Report TC 211-PAE, Springer, Dordrecht, 2013, pp. 131-173.

2. C. Carde and R. François, Effect of the leaching of calcium hydroxide from cement paste on mechanical and physical properties, Cement Concrete Res. 27 (1997) 539-550.

3. K.L. Scrivener, J-.L. Cabiron and R. Letourneux, High-performance concretes from calcium aluminate cements, Cement Concrete Res. 29 (1999) 1215–1223.

4. Y.H. Kim, Basic iron (III) alkanoate complexes, Masters Theses, Missouri University of Science and Technology, Rolla, 1967.

5. O. Ye´pez, On the chemical reaction between carboxylic acids and iron, including the special case of naphthenic acid, Fuel 86 (2007) 1162–1168.

6. W.M. Haynes, CRC Handbook of Chemistry and Physics, 95th ed., CRC Press, Boca Raton, 2014.

7. A.E. Martell and R.M. Smith, Critical Selected Stability Constants of Metal Complexes Database, Version 6.0 for Windows, National Institute of Standards and Technology, Gaithersburg, 2004.

8. C. Saury, R. Boistelle, F. Dalemat and J. Bruggeman, Solubilities of calcium acetates in the temperature range 0-100°C, J. Chem. Eng. Data 38 (1993) 56-59.

9. E.A. Klop, A. Schouten, P. van der Sluis and A.L. Spek, Structure of calcium acetate monohydrate, $Ca(C_2H_3O_2)_2.H_2O$, Acta Crystallogr. C 40 (1984) 51-53.

10. C. Balarew, D. Stoilova and L. Demirev, Untersuchung einiger dreistoffsysteme vom typ $Me(OCOCH_3)_2 – CH_3COOH – H_2O$ bei 25°C (Me = Ni, Co, Mg, Mn, Ca), Z. Anorg. Allg. Chem. 410 (1974) 75-87.

11. E.A. Klop and A.L. Spek, Structure of calcium hydrogen triacetate monohydrate, $CaH(C_2H_3O_2)_3.H_2O$, Acta Crystallogr. C 40 (1984) 1817-1819.

12. R.J. Lewis, Hawley's Condensed Chemical Dictionary, 15th ed, Wiley-Interscience, Hoboken, 2007.

13. R. Alcala and J.F. Garcia, Determinacion de las estructuras cristalinas de los acetatos de hierro y cobalto, Revista de la Academia de Ciencias Exactas, Fisico-Quimicas y Naturales de Zaragoza 28 (1973) 303-325.

14. A. Seidell, Solubilities of Inorganic and Organic Compounds, 2nd ed. Van Nostrand, New York, 1919.

15. A. Valora, E. Reguera and F. Sanchez-Sinencio, Synthesis and X-ray diffraction study of calcium salts of some carboxylic acids, Powder Diffr. 17 (2002) 13-18.

16. L. Lutterotti, Total pattern fitting for the combined size-strain-stress-texture determination in thin film diffraction, Nucl. Instrum. Meth. B 268 (2010) 334-340.

17. D.L. Parkhurst and C.A.J. Appelo, Description of input and examples for PHREEQC version 3 – A computer program for speciation, batch-reaction, one-dimensional transport, and inverse geochemical calculations. In U.S. Geological Survey Techniques and Methods, Book 6, Chapter A43. US Geological Survey, Denver, 2013. See http://pubs. usgs.gov/tm/06/a43 (accessed 23/11/2016).

18. S.R. Charlton and D.L. Parkhurst, Modules based on the geochemical model PHREEQC for use in scripting and programming languages, Computers & Geosciences 37 (2011) 1653-1663.

19. T. Dyer, Influence of cement type on resistance to organic acids, Mag. Concrete Res. (in press) (2016).

20. U.S. Environmental Protection Agency, MINTEQA2/PRODEFA2, A geochemical assessment model for environmental systems—User manual supplement for version 4.0: National Exposure Research Laboratory, Athens, GA, 1999.

21. B. Lothenbach, T. Matschei, G. Möschner and F.P. Glasser, Thermodynamic modelling of the effect of temperature on the hydration and porosity of Portland cement. Cement Concrete Res. 38 (2008) 1–18.

22. L. De Windt and P. Devillers, Modeling the degradation of Portland cement pastes by biogenic organic acids, Cement Concrete Res. 40 (2010) 1165–1174.

23. Stronach SA, Glasser FP, Modeling the impact of abundant geochemical components on phase stability and solubility of the $CaO–SiO_2–H_2O$ systems at 25 °C: Na^+, K^+, SO_4^{2-}, Cl^- and CO_3^{2-}, Adv. Cem. Res. 9 (1997) 167–181.

24. F.P. Glasser, Chemistry of cement-solidified waste forms, R.D. Spence (Ed.), Chemistry and Microstructure of Solidified Waste Forms, Lewis Publishers, Boca Raton, 1992, pp. 1-39.

25. D.V. Chapman, Water Quality Assessments: A guide to the use of biota, sediments and water in environmental monitoring, 2nd ed., Taylor and Francis, London, 1996.

26. Pavlík, V, Corrosion of hardened cement paste by acetic and nitric acids. Part II: formation and chemical composition of the corrosion products layer. Cement and Concrete Res. 24 (1994) 1495-1508.